Materials Transactions, Vol. 57, No. 6 (2016) pp. 781 to 788
Special Issue on Advanced Spintronic/Nano-Magnetic Materials

Perpendicular Exchange Bias and Magneto-Electric Control Using Cr_2O_3(0001) Thin Film

Yu Shiratsuchi* and Ryoichi Nakatani

Graduate School of Engineering, Osaka University, 2–1 Yamada-oka, Suita, Osaka 565–0871, Japan

Antiferromagnets themselves do not generate either stray fields or spontaneous magnetization. However, if an antiferromagnet is coupled with a ferromagnet, unique and useful characteristics appear. Exchange bias is one such characteristic that is utilized in spintronic devices like spin-valve films. To date, exchange bias has been used to induce static effects in devices; however, the exchange bias has not been switchable in these devices. Recently, switchable exchange bias has been developed using Cr_2O_3, which exhibits a magnetoelectric effect in an antiferromagnetic layer. The promising features of this effect are (1) the strength of the exchange bias is high and its direction is perpendicular to the film, and (2) the switching is triggered by an electric field. In this overview, we will summarize our recent results on the unique temperature dependence of high, perpendicular exchange bias and magnetoelectric switching of the induced perpendicular exchange bias.
[doi:10.2320/matertrans.ME201506]

(Received January 14, 2016; Accepted March 14, 2016; Published April 15, 2016)

Keywords: *perpendicular exchange bias, Cr_2O_3 thin film, magnetoelectric effect, antiferromagnet, interfaces*

1. Introduction

Control of the direction of magnetization is a key requirement of spintronic and magnetic devices. The magnetization direction of a ferromagnetic (FM) material can be easily adjusted by using a magnetic field or a spin-polarized current[1,2] because FM materials possess spontaneous magnetization. In contrast, in an antiferromagnetic (AFM) material, the spins are fully compensated and spontaneous magnetization is not generated; thus, the spins of AFM materials have been difficult to control in devices. In fact, in conventional devices, AFM materials are used to fix the magnetization directions of FM materials by inducing exchange bias[3]; thus, AFM materials have been employed to induce static effects. If the exchange bias in a device can be switched, a new method of controlling spin as well as expanded functionality of spin-valve films can be realized.

Cr_2O_3 is an oxide AFM material that exhibits the magnetoelectric (ME) effect[4,5]. In this effect, electric polarization is induced by a magnetic field[4], and conversely, magnetization is induced by an electric field[5]. Notably, when magnetic and electric fields are applied simultaneously, the directions of the induced electric polarization and magnetization are controllable. The ME effect was predicted by Pierre Curie in 1894[6], and in 1960, Dzyaloshinskii proposed that Cr_2O_3 was likely to exhibit this phenomenon[7]. In Fig. 1, the crystal structure and spin alignment of Cr^{3+} in Cr_2O_3 are shown schematically. Cr_2O_3 has a corundum structure in which the Cr^{3+} spins are aligned along the *c*-axis and are antiferromagnetically coupled in the adjacent layer[8–10]. This AFM ordering breaks time-reversal symmetry, and in addition, at the Cr^{3+} ion site in the corundum structure, spatial inversion symmetry is broken. Because of these two simultaneous symmetry breaks, Cr_2O_3 exhibits the ME effect.

Although the theoretical prediction was experimentally confirmed soon after the prediction by Dzyaloshinskii[4,5], the ME effect exhibited by Cr_2O_3 was applied in spintronic devices only in 2005, by Borisov *et al.*[11]. They employed the ME phenomenon to control exchange bias electrically and demonstrated that the exchange bias in a $[Pd/Co]_3/Pd/Cr_2O_3$-substrate stacked system is controllable by an electric field. At that time, the ME effect was still induced using bulk Cr_2O_3, and its demonstration in an all-thin-film system was reported only very recently[12,13]. As long as the ME effect of Cr_2O_3 is caused by the interaction between the crystal structure and the spin alignment, high crystalline quality, suitable AFM ordering, and sufficient Cr_2O_3 thin film resistivity are

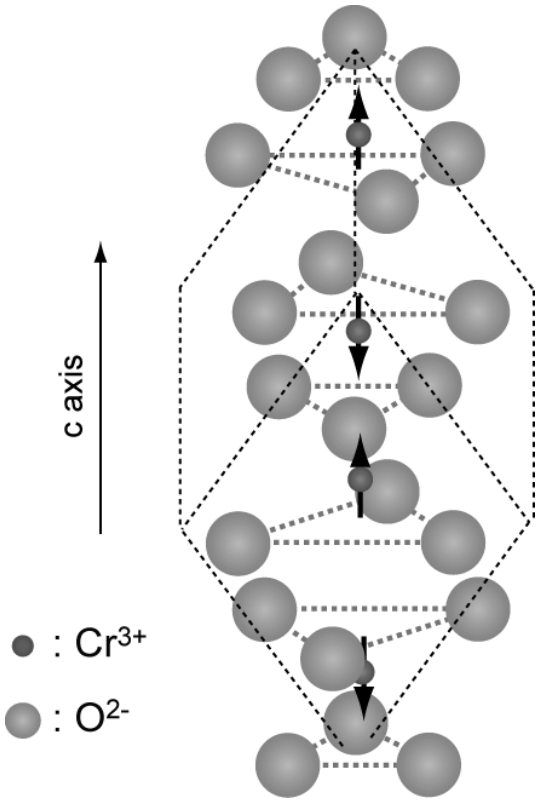

Fig. 1 Crystal structure and spin alignment of Cr^{3+} in Cr_2O_3.

*Corresponding author, E-mail: shiratsuchi@mat.eng.osaka-u.ac.jp

essential to realize the ME phenomenon in an all-thin-film system; however, achieving these characteristics remains non-trivial.

In this paper, we review the previous reports on ME-controlled exchange bias in all-thin-film systems with Cr_2O_3 layers, focusing mainly on our own achievements[13–18]. We also discuss the characteristics of the exchange bias achieved using Cr_2O_3 thin films because it has been hypothesized that exchange bias can be induced by using this material, and exchange bias itself is of significant interest in the field of nano-magnetism. In chapter 2, we show that the exchange bias induced by a $Cr_2O_3(0001)$ thin film exhibits (1) high, perpendicular exchange anisotropy above 0.4 mJ/m^2 and unique temperature dependence, with abrupt onset at a specific temperature, as well as (2) a close relationship with the boundary magnetization, which is coupled with the ME effect. In chapter 3, we present two methods of switching the ME-controlled exchange bias: ME field cooling (MEFC)[11–13] and isothermal switching[16,19,20]. In chapter 3, we also address dynamic exchange bias reversal by using a pulsed voltage.

2. Perpendicular Exchange Bias Induced by $Cr_2O_3(0001)$ Thin Film

2.1 High, perpendicular exchange bias and its unique temperature dependence

Future spintronic/magnetic devices should be capable of high integration, low power consumption, and high-speed operation, among other requirements. To realize these characteristics, it is commonly considered that the spin orientation should be perpendicular to the film, unlike in a conventional in-plane magnetized system. This paradigm shift is required not only for the FM/AFM spin orientation, but also for the exchange bias direction; that is, perpendicular exchange bias is also required. Since the Cr^{3+} spins are aligned along the *c*-axis of the corundum structure (Fig. 1), it is expected that the AFM spin orientation is restricted to the direction perpendicular to the film and that perpendicular exchange bias can therefore be induced by aligning the *c*-axis of the Cr_2O_3 thin film along the surface normal.

We previously reported that, by appropriately choosing the substrate and buffer layer, a $Cr_2O_3(0001)$ layer could be grown easily using conventional sputtering techniques and that subsequent layers were grown epitaxially on the $Cr_2O_3(0001)$ layer[14]. A typical magnetization curve exhibiting perpendicular exchange bias, measured using the polar magneto-optic Kerr effect (MOKE), is shown in Fig. 2. This curve was obtained by using a Pt(111)/Co(111)/$Cr_2O_3(0001)$/Pt(111) stacked film. The out-of-plane magnetization component is observable in the polar MOKE; thus, the exchange bias shown in Fig. 2 agrees with the above prediction. The exchange anisotropy energy J_K, defined as $J_K = M_S \cdot t_{FM} \cdot H_{EX}$ (where M_S is the saturation magnetization, t_{FM} is the FM layer thickness, and H_{EX} is the exchange bias field), can exceed 0.4 mJ/m^2 [15]. Perpendicular exchange bias has been reported in several systems using other AFM layers such as CoO[21], NiO[22], FeF_2[23], MnPd[24], Fe-Mn[25–27], and Ir-Mn[26,28–31]. The J_K values of such systems have been reported to be 0.31 mJ/m^2 at 10 K for (Co+CoO)(15 nm)/[Pt(0.5 nm)/Co(0.4 nm)]$_5$[21], ~0.17 mJ/m^2 at 120 K for [MnPd(10 nm)/Co(10 nm)]$_{10}$ multilayer[24], and ~0.4 mJ/m^2 at room temperature for [Pt(1 nm)/Co(0.6 nm)]$_4$/Pt(1 nm)/$Fe_{40}Co_{60}$(1.2 nm)/Ir-Mn(5 nm)[31]. Thus, J_K is relatively high for the Pt/Co/Cr_2O_3/Pt film, and it is comparable to that of the film containing Ir-Mn. High J_K values in films containing Ir-Mn have been achieved by inserting suitable spacer layers such as Pt[25,26] and Fe-Co[30,31] between their Pt/Co multilayers and Ir-Mn layers. This is because that when the Pt/Co multilayer is directly deposited on the Ir-Mn layer, the in-plane interface magnetic anisotropy was induced[28]. The in-plane interface magnetic anisotropy at an FM/AFM interface tends to cant the interfacial spins away from the surface normal. In order to suppress this effect, a suitable spacer layer can be inserted to induce interface perpendicular magnetic anisotropy[29], implying that collinear spin alignment along the normal to the FM/AFM interface is sufficient to induce high, perpendicular exchange anisotropy. This effect can be simply predicted by the fact that the exchange coupling energy is proportional to the scalar product of the FM and AFM spins. Thus, the relatively high J_K value observed in the Pt/Co/Cr_2O_3/Pt film can be understood as having been partly caused by the Cr^{3+} spins being aligned perpendicular to the film at the $Cr_2O_3(0001)$ surface. In addition, unlike in the [Pt/Co]-multilayer/Ir-Mn film, the perpendicular magnetic anisotropy at the Co/Cr_2O_3 interface[32] would also contribute the high J_K value.

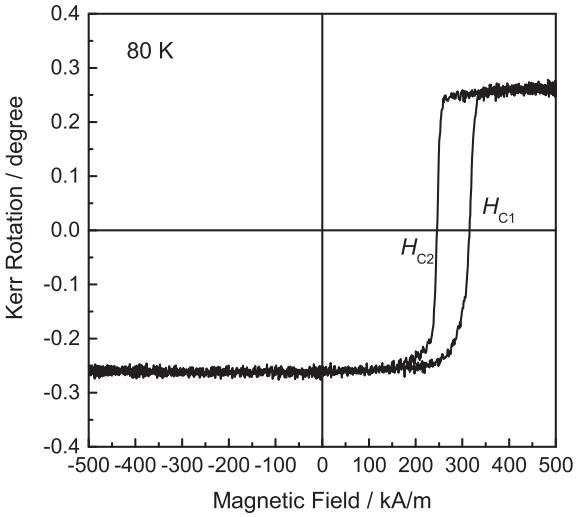

Fig. 2 Typical polar MOKE loop exhibiting perpendicular exchange bias in Pt(5 nm)/Co(0.8 nm)/Cr_2O_3(70 nm)/Pt(20 nm) stacked film.

The perpendicular exchange bias, induced by the $Cr_2O_3(0001)$ thin film, exhibits unique temperature dependence[14]. Figure 3(a) shows the variation of the coercivity with temperature. In the figure, the coercivities H_{C1} and H_{C2} defined in Fig. 2 for the increasing and decreasing branches of the magnetization curve, respectively, are shown separately. The measurements were performed after the sample was cooled in a magnetic field of −4 kOe. The absolute values of H_{C1} and H_{C2} increase with decreasing temperature, and at 122 K, H_{C2} abruptly increases and changes sign. Since $H_{EX} = (H_{C1} - H_{C2})/2$, this abrupt change indicates the abrupt onset of exchange bias, as shown in Fig. 3(b). In Fig. 3(b), it is also evident that the coercivity $H_C = (H_{C1} + H_{C2})/2$ abruptly decreases at the H_{EX} onset temperature and that the amount of

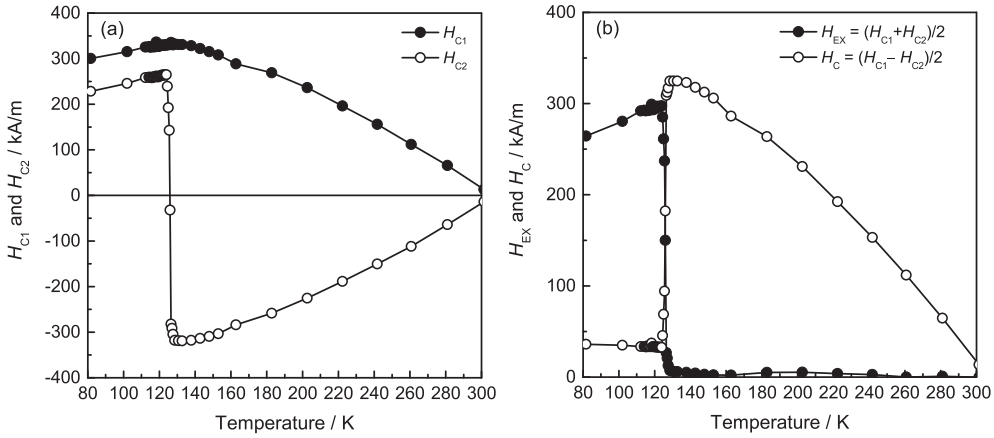

Fig. 3 Temperature dependences of (a) H_{C1} and H_{C2} and (b) H_{EX}. Definitions of H_{C1} and H_{C2} are shown in Fig. 2.

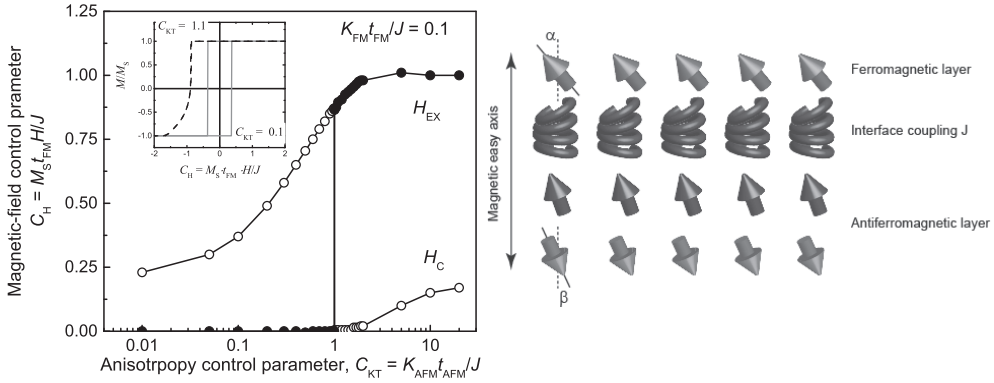

Fig. 4 (left) Calculated changes of C_H (= $M_S \cdot t_{FM} \cdot H/J$) with C_{KT} (= $K_{AFM} \cdot t_{AFM}/J$). (right) Supposed spin configurations.

decrease, ΔH_C, is exactly equal to H_{EX} at that temperature.

In the Mn-based system, the above-mentioned critical condition for the appearance of H_{EX} was rarely observed in the AFM layer thickness dependence of H_{EX}[33,34] and was not evident at all in its temperature dependence. Instead, the temperature dependences of H_{EX} in other exchange-biased systems have often shown that H_{EX} gradually decreases with increasing temperature and finally becomes zero at the blocking temperature[35–39]. This trend occurs because the thermal agitation of the AFM magnetization dominates the temperature dependence of the exchange bias.

The abrupt onset of H_{EX} and the quantitative relationship $H_{EX} = \Delta H_C$ at the onset temperature are predicted by the simple model developed by Meiklejohn and Bean, termed the M-B model[33,34,40]. The total magnetic energy density per unit area of an FM/AFM stacked system is expressed as

$$tE = -M_S \cdot t_{FM} \cdot H \cdot \cos\alpha + (K_{FM} - 2\pi M_S^2) \cdot t_{FM} \cdot \sin^2\alpha + K_{AFM} \cdot t_{AFM} \sin^2\beta - J\cos(\alpha - \beta), \quad (1)$$

where t is the total thickness, H is the external magnetic field, K_{FM} is the magnetic anisotropy of the FM layer, K_{AFM} is the magnetic anisotropy of the AFM layer, t_{AFM} is the AFM layer thickness, J is the interfacial exchange coupling energy, and α and β denote the angles of the FM and AFM spins, respectively, from the surface normal (see Fig. 4). The first and second terms represent the Zeeman energy and the magnetic anisotropy energy of the FM layer, respectively. In the case of an in-plane exchange-biased system, K_{FM} can sometimes be neglected because the FM layer is often polycrystalline, and the magnetic easy axes are therefore randomly dispersed in the film plane. Furthermore, magnetic anisotropy is not required to express the in-plane magnetization of the FM layer correctly if the demagnetization field, $-2\pi M_S^2$, is considered[33,34]. However, in the case of a perpendicular exchange-biased system, it is necessary to use K_{FM} to express the perpendicular magnetic anisotropy of the FM layer correctly; otherwise, the magnetization would lie in the film plane because of the strong in-plane demagnetization field. The third term is the magnetic anisotropy of the AFM layer, and the last term represents the interfacial exchange coupling between the FM and AFM spins. Based on previous reports on in-plane exchange-biased systems[33,34], for our analysis, we also defined a reduced anisotropy control parameter C_{KT} according to

$$C_{KT} = K_{AFM} \cdot t_{AFM}/J \quad (2)$$

and a reduced magnetic-field control parameter C_H according to

$$C_H = M_S \cdot t_{FM} \cdot H/J. \quad (3)$$

C_{KT} and C_H are dimensionless parameters reflecting the magnetic anisotropy energy density of the AFM layer per unit area and the magnetic field, respectively. C_H can express either the exchange bias or the coercivity by using H_{EX} or H_C, respectively, as H in eq. (3). Using eq. (1), the magnetization curves for the various values of C_{KT} were calculated. Then, the obtained C_H values were plotted versus C_{KT}, as shown in

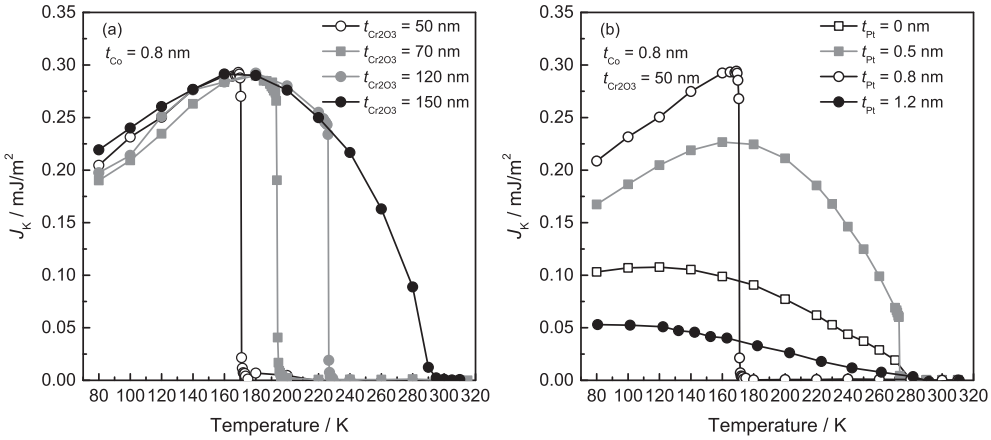

Fig. 5 Temperature dependences of exchange bias field for films possessing (a) different Cr_2O_3 layer thicknesses[14] and (b) different Pt spacer layer thicknesses[41], i.e., with different interfacial exchange coupling energies.

Fig. 4. When $C_{KT} = 1$, the exchange bias appears, and the coercivity diminishes abruptly. If $C_{KT} < 1$, the AFM spins reverse together with the FM spins. In this case, the exchange anisotropy appears as a coercivity enhancement. However, when $C_{KT} > 1$, the AFM spin direction is fixed even when the FM spin is reversed because the magnetic anisotropy of the AFM layer overcomes the interfacial exchange coupling.

Based on this simple discussion, the temperature dependences of H_{EX} and H_C that are shown in Fig. 3 can be explained by assuming that K_{AFM}/J changes with temperature. Based on the above criterion for the appearance of H_{EX}, i.e., $C_{KT} = 1$, the onset temperature of H_{EX} is expected to increase with increasing t_{AFM} or with decreasing J. This prediction was qualitatively confirmed by varying t_{AFM}[14] (Fig. 5(a)) and J by inserting Pt spacer layers with different thicknesses[41] (Fig. 5(b)). However, the quantitative validity of the H_{EX} onset criterion has not been verified with absolute certainty, partly because the above model is based on the coherent rotation of the FM spin reversal and because the AFM spins are constant in spite of the FM spin reversal. In fact, a linear relationship between $K_{AFM} \cdot t_{AFM}$ and J_K was not obtained at the onset temperature, as shown in Fig. 6. The data presented in Fig. 6 were acquired using various samples possessing different t_{AFM} and J_K, and the K_{AFM} value at the onset temperature was estimated from the reported bulk value[42]. In order to explain the onset temperature quantitatively, further investigations including the determination of K_{AFM} in collaboration with theoretical calculations are necessary.

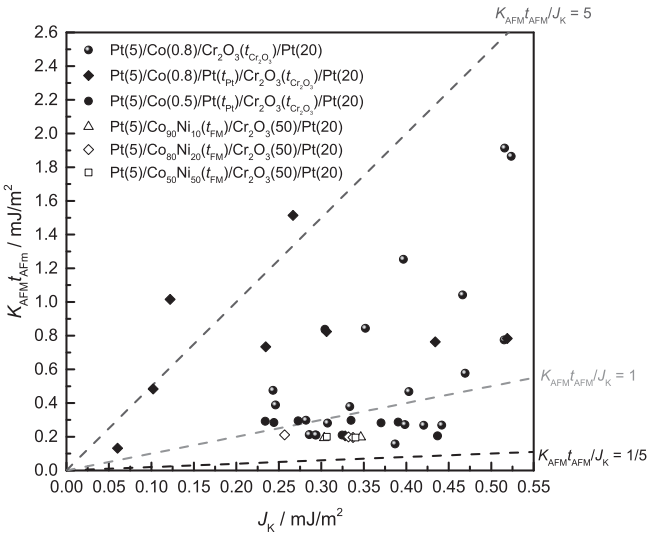

Fig. 6 Relationship between $K_{AFM} \cdot t_{AFM}$ and J_K at onset temperature for various films possessing different J_K and t_{AFM}. K_{AFM} at onset temperature was estimated from bulk value[42].

2.2 Perpendicular exchange bias and boundary magnetization on Cr_2O_3(0001) surface

Exchange anisotropy is induced by interfacial exchange coupling between the FM and AFM spins, and exchange bias is observed because of the unidirectional nature of this exchange anisotropy. This unidirectional nature requires some symmetry breaking of the interfacial spin structure. Interfacial uncompensated AFM spins can cause this symmetry breaking, and substantial effort has been devoted to determining their origin[43,44] and their quantitative relationship with J_K[45,46]. On Mn-Ir(111) surfaces, which have been intensively studied, the interface Mn spins are fully compensated unless the Mn-Ir is exchange-coupled with the FM layer. Furthermore, in in-plane exchange-biased systems such as Co-Fe/IrMn(111) film, it has been shown that uncompensated Mn spins can be induced by spin canting from the original direction due to exchange coupling with the FM spins[44]. The canting angle, which is proportional to the amount of uncompensated AFM spin, increases with increasing interfacial exchange coupling strength. Hence, J_K is proportional to the amount of interfacial uncompensated AFM spin[45]. In contrast, the interfacial uncompensated AFM spin amount in a Pt/Co/Cr_2O_3 perpendicular exchange-biased system is closely related to the boundary magnetization on the Cr_2O_3(0001) surface. This boundary magnetization was first advocated by Andereev in 1996[47], and more recently by Belashckenko in 2010[48]. They predicted, based on symmetry arguments, that the boundary of an ME AFM layer such as Cr_2O_3 has an equilibrium magnetization. The boundary magnetization can be detected using surface-sensitive spin-polarized probes such as X-ray magnetic circular dichroism (XMCD)[13,49]. In a Pt/Co/Cr_2O_3 thin film, clear XMCD signals could be detected at both the Co L_3 and Cr L_3 edges, as shown in Fig. 7 (a), and

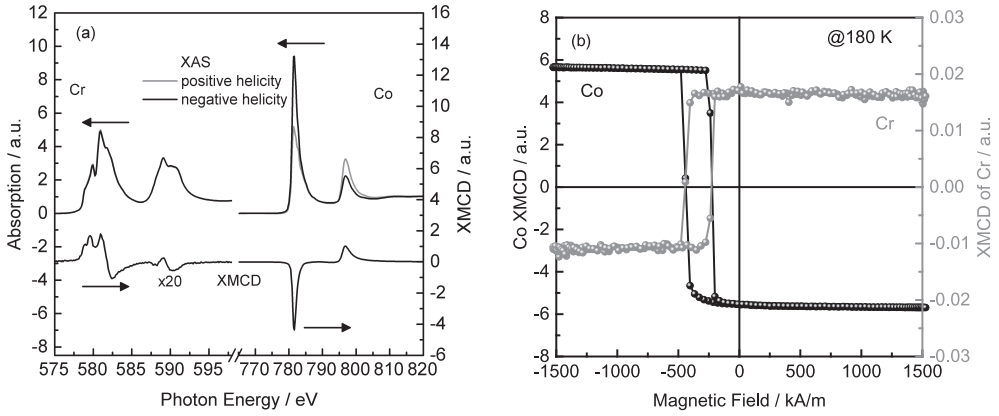

Fig. 7 (a) Soft X-ray absorption spectra and XMCD spectra at Co L_3 and Cr L_3 edges. (b) Element-specific magnetization curves for Co and Cr[15].

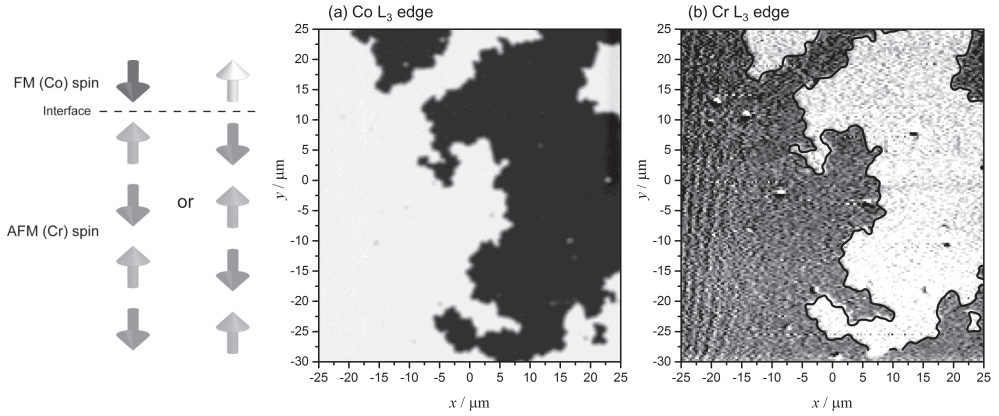

Fig. 8 Spatial distributions of XMCD intensity measured at (a) Co L_3 edge and (b) Cr L_3 edge corresponding to FM and AFM domains, respectively[18] Colors correspond to spin orientations schematically shown at left. Solid line in (b) represents domain boundary of FM layer.

the Cr XMCD signal was found to reverse when the Co spin was reversed (Fig. 7(b)). Thus, the induced boundary magnetization is exchange-coupled with the FM spin. The results shown in Fig. 7 also reveal that the Co and Cr spins are antiferromagnetically coupled because the signs of their XMCD signals are opposite. Furthermore, the Cr XMCD signal could be detected by the surface-sensitive total electron yield method, but not by the bulk-sensitive transmission method[13], indicating that the uncompensated AFM spins were localized at the Co/Cr_2O_3 interface; these results agree with the boundary magnetization mechanism. It should be noted that for the Cr_2O_3(0001) thin film alone, no Cr XMCD signal was detected[13], because the magnetic domains that possess oppositely directed boundary magnetizations are energetically degenerate and because the boundary magnetization, i.e., the interfacial uncompensated AFM spins are not macroscopically detectable. In contrast to the Co-Fe/Mn-Ir(111) in-plane exchange-biased system, the XMCD intensities at Cr $L_{2,3}$ edges are similar for films possessing different interface roughnesses and J_K values[13]. These characteristics also agree with the theoretical prediction that the boundary magnetization is roughness-insensitive and in an equilibrium state[48].

The boundary magnetization and J_K are not coupled; however, the boundary magnetization direction is coupled with the exchange bias polarity[15,18,19]. Figure 8 shows the spatial distributions of the XMCD intensities measured at the Co L_3 and Cr L_3 edges, which correspond to the FM and AFM domains, respectively, at 265 K after cooling the sample in zero magnetic field to maintain the demagnetized state[18]. It can be seen that the FM and AFM domain patterns are spatially similar, indicating that the FM and AFM layers are exchange-coupled on a domain-by-domain basis. Furthermore, the magnetization curves after zero-field cooling exhibit exchange bias fields with both positive and negative directions, indicating that the polarity of the exchange bias is determined on a domain-by-domain basis. Spatial coupling of FM and AFM domains has also been reported in a Co/$LaFeO_3$ in-plane exchange-biased system[50].

3. Magnetoelectric Switching of Perpendicular Exchange Bias in All-Thin-Film Systems

Martin and Anderson[51] derived the free energy of an ME substance under magnetic and electric fields as

$$F_{\pm} = F_0 + \sigma_i H_i + \rho_i E_i + 1/2\chi_{ij} H_i H_i + 1/2\chi'_{ij} E_i E_i \pm \alpha_{ij} E_i H_j + \cdots , \quad (4)$$

where the first term is a constant. The second and third terms represent the pyromagnetism and the pyroelectric polarization, respectively, which can be eliminated for Cr_2O_3 because of the crystallographic symmetry. The fourth and fifth terms represent the magnetization and the electric polarization, respectively, and the sixth term represents the ME effect. F_+ and

F_- denote the free energies of the oppositely directed AFM spins. Equation (4) indicates that an energy difference that can be expressed as

$$\Delta F = 2\alpha_{ij}E_iH_j \quad (5)$$

is generated for oppositely directed AFM domains. In other words, by applying magnetic and electric fields simultaneously, i.e., if H and E are both non-zero, the AFM domains are switchable[11–13,16,17,19,20,51]. Since the polarity of the perpendicular exchange bias in a Pt/Co/Cr_2O_3/Pt system is determined by the interfacial AFM spin orientation, the exchange bias can be made switchable by using the ME effect. Figure 9 shows an example of the change in the exchange bias polarity achieved by simultaneously applying magnetic and electric fields. To obtain this figure, a Pt(5 nm)/Co(0.8 nm)/Pt(0.5 nm)/Cr_2O_3(150 nm)/Pt(20 nm) stacked film was used. Upon polarity reversal, H is constant in both polarity and strength; thus, the exchange bias polarity reversal was caused by the reversal of E. To date, two types of ME-induced switching have been proposed: MEFC switching[11–13] and isothermal switching[16,19,20]. In the following sections, we describe the microscopic mechanisms of these two switching modes.

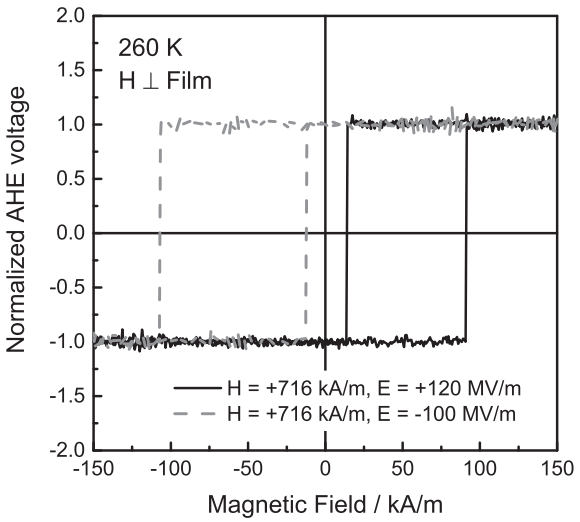

Fig. 9 Typical magnetization curve measured by anomalous Hall effect after applying ME fields. Solid black and dashed gray curves represent curves after applying H = +716 kA/m, E = +120 MV/m and H = +716 kA/m, E = −100 MV/m, respectively[17].

3.1 Magnetoelectric field cooling mode

In general, exchange bias is induced by cooling a sample from above the Néel temperature in a magnetic field, which is known as the field-cooling process. MEFC is, in contrast, a cooling process in which magnetic and electric fields are applied simultaneously during cooling[11]. In MEFC, the polarity of the exchange bias is determined by the sign and amplitude of the product of H and E, i.e., the EH product. Figure 10(a) shows the change in H_{EX} with E during MEFC for a Pt(5 nm)/Co(0.8 nm)/Cr_2O_3(200 nm)/Pt(20 nm) thin film. H was kept constant in the range of 8 kOe to 10 kOe during the MEFC process. Below the threshold value of E, H_{EX} is negative, similarly to in the conventional field cooling process, because of the positive value of H. When E increases to above its threshold value, H_{EX} changes sign from negative to positive. In the figure, it is also apparent that the threshold value of E increases with decreasing H. We defined the threshold value of E as that at which H_{EX} becomes zero. The variation of the threshold value of E with H is shown in Fig. 10(b). The threshold value of E is inversely proportional to H, indicating that the EH product is constant at the threshold, which agrees with the ME mechanism described above. In Fig. 10(b), the results for films with different J_K are plotted. The J_K values presented in Fig. 10(b) were calculated using H_{EX} at a measurement temperature of 265 K. J_K can be altered by changing the crystalline quality of Cr_2O_3[13] or by inserting a Pt spacer layer between the Co and Cr_2O_3 to change the interfacial exchange coupling strength[41] (also see Fig. 5(b)). The slope of each line in Fig. 10(b) corresponds to the EH product required to switch the exchange bias polarity. It is likely that the slope increases with increasing J_K, so a higher EH product is required for films possessing higher J_K. This observation can be qualitatively interpreted as the energy competition between the interfacial exchange coupling energy and the energy gain by the ME effect[17]. Below the threshold value of the EH product, the interface exchange coupling with the FM spins determines the direction of the interfacial AFM spins. In this case, the polarity of the exchange bias is determined by the magnetic field direction, as in the conventional field cooling process. When the EH prod-

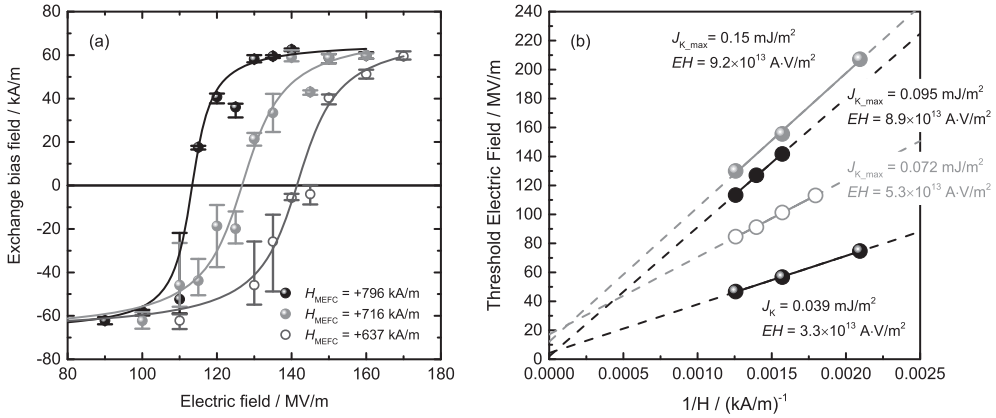

Fig. 10 (a) Change in H_{EX} with E during MEFC. H applied during MEFC was +796 kA/m (black), +716 kA/m (dark gray), and +637 kA/m (dark gray). Solid lines are guides to eye. (b) Variation of threshold value of E with H during MEFC.

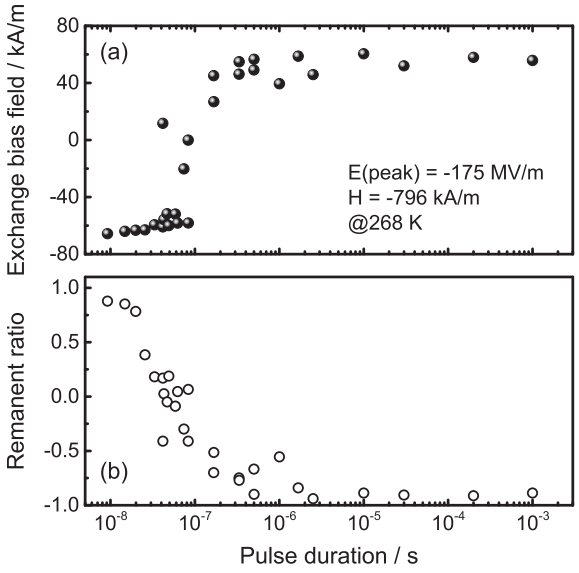

Fig. 11. Changes in (a) H_{EX} and (b) remanence ratio with voltage pulse duration at 268 K[16].

uct exceeds the threshold value, the energy gain due to the ME effect overcomes the interfacial exchange coupling energy; then, the direction of the interfacial AFM spins is determined by the ME effect.

Obviously, exchange bias polarity reversal occurred when the above-mentioned energy competition actually occurs. On the other hand, when the electric field was applied in the opposite direction, both the ME effect and the interfacial exchange coupling induce exchange bias with the same polarity, and exchange bias polarity reversal does not occur.

Although the energy competition between the ME effect and the interfacial exchange coupling qualitatively explains the results, quantitative interpretation is a non-trivial problem. One difficulty lies in determining the interfacial exchange coupling energy because it is not equal to J_K, as has been intensively discussed since the discovery of exchange anisotropy[40].

3.2 Isothermal switching mode

The MEFC mode requires temperature hysteresis to switch the exchange bias polarity, and switching occurs upon formation of the AFM order. Thus, this process yields the minimum *EH* product for a film. MEFC could be useful, for example, for heat-assisted magnetic recording[52]. In contrast, isothermal switching occurs at a constant temperature, as its name suggests. In addition to this important engineering difference, isothermal switching enables us to access the dynamics of switching with pulsed voltages[16]. Figure 11 shows the changes in H_{EX} and remanence ratio with the duration of the input voltage pulses. The film used to obtain Fig. 11 was identical to that used for Fig. 10(a). In the measurements, the temperature was maintained at 268 K, and H was held constant at -796 kA/m during the voltage application. The amplitude of the pulsed voltage was -35 V, which corresponds to $E = -175$ MV/m. The input *EH* product was therefore approximately 1.3 times higher than the threshold *EH* product of $\sim -1.1 \times 10^{14}$ A·V/m^2 at this temperature. As shown, H_{EX} increases and the remanence ratio decreases gradually with increasing pulse duration. The time required to complete the switching process is 200–300 ns under these conditions. This switching time is very long compared with the precession time of the FM and AFM spins, which is typically in the sub-nanosecond range[53]. The slow switching implies that the switching process is dominated by magnetic domain wall motion. According to reports on magnetic domain wall dynamics examined using FM wires, the magnetic domain wall velocity depends on the input energy density[54], and it is expected that the switching time of our investigated system could be decreased by increasing the input *EH* product. The variation of the switching time with the input *EH* product is now under investigation.

In principle, it would be possible to determine the AFM domain wall mobility from this type of measurement, using a method similar to that employed for FM wires[55,56]. However, the domain wall propagation direction is more difficult to determine in AFM materials than in FM wires. Hence, direct observations of the magnetic domain structure changes after applying pulsed fields are necessary, and we are now investigating this type of measurement.

4. Concluding Remarks

Recent progress in investigations of perpendicular exchange bias using Cr_2O_3 as an AFM material and its ME functionality were reviewed in this report. This overview is mainly dedicated to the achievements of our research group because ME control of perpendicular exchange bias is a new field in which we have been very active since the first report of this phenomenon in an all-thin-film system. This pioneering work has led to increasing research in the field of ME control of AFM spin. Together with these recent developments, experimental techniques such as AFM domain imaging using focused soft/hard X-rays will help understanding of the underlying physics. The authors believe that these characterization techniques will contribute to achieving the requirements of advanced spintronics and hope to establish a community in this research field.

Acknowledgments

The authors would like to thank Dr. Chiharu Mitsumata of the National Institute of Materials Science (NIMS) for valuable discussions; Dr. Tetsuya Nakamura, Dr. Motohiro Suzuki, Dr. Toyohiko Kinoshita, and Dr. Yoshinori Kotani of the Japan Synchrotron Radiation Research Institute (JASRI) for the XAS/XMCD measurements; and Dr. Hikaru Nomura and Dr. Kentaro Toyoki (present affiliation, JASRI/SPring-8) of Osaka University for support performing the ME measurements.

The XAS/XMCD measurements were performed at the SPring-8 synchrotron radiation facility with the approval of JASRI (Proposal Nos. 2011A1172, 2014A0069, 2014B0079, 2015A0079, and 2015B0079). This work was partly supported by the ImPACT program, JSPS KAKENHI (Grant Nos. 26630296 and 25706007), the Photonics Advanced Research Center (PARC) at Osaka University, and the Izumi Science and Technology Foundation.

REFERENCES

1) L. Berger: Phys. Rev. B **54** (1996) 9353–9358.
2) J.C. Slonczewski: J. Magn. Magn. Mater. **159** (1996) L1–L7.
3) B. Dieny, V.S. Speriousu, S.S.P. Parkin, B.A. Gurney, D.R. Wilhoit and D. Mauri: Phys. Rev. B **43** (1991) 1297–1300.
4) D.N. Astrov: Sov. Phys. JETP **11** (1960) 708–709.
5) V.J. Folen, G.T. Rado and E.W. Staldar: Phys. Rev. Lett. **6** (1961) 607–608.
6) P. Curie: J. Phys. Paris **3** (1894) 393–415.
7) I.E. Dzyaloshinskii: J. Exp. Theor. Phys. **10** (1960) 628–629.
8) B.N. Brockhouse: J. Chem. Phys. **21** (1953) 961–962.
9) G.W. Pratt, Jr. and P.T. Bailey: Phys. Rev. **131** (1963) 1923–1928.
10) L.M. Corliss, J.M. Hastings, R. Nathans and G. Shirane: J. Appl. Phys. **36** (1965) 1099–1100.
11) P. Borisov, A. Hochstrat, X. Chen, W. Kleemann and C. Binek: Phys. Rev. Lett. **94** (2005) 117203.
12) T. Ashida, M. Oida, N. Shimomura, T. Nozaki, T. Shibata and M. Sahashi: Appl. Phys. Lett. **104** (2014) 152409.
13) K. Toyoki, Y. Shiratsuchi, T. Nakamura, C. Mitsumata, S. Harimoto, Y. Takechi, T. Nishimura, H. Nomura and R. Nakatani: Appl. Phys. Express **7** (2014) 114201.
14) Y. Shiratsuchi, T. Fujira, H. Oikawa, H. Noutomi and R. Nakatani: Appl. Phys. Express **3** (2010) 113001.
15) Y. Shiratsuchi, H. Noutomi, H. Oikawa, T. Nakamura, M. Suzuki, T. Fujita, K. Arakawa, Y. Takechi, H. Mori, T. Kinoshita, M. Yamamoto and R. Nakatani: Phys. Rev. Lett. **109** (2012) 077202.
16) K. Toyoki, Y. Shiratsuchi, A. Kobane, C. Mutsumata, Y. Kotani, T. Nakamura and R. Nakatani: Appl. Phys. Lett. **106** (2015) 162404.
17) K. Toyoki, Y. Shiratsuchi, A. Kobane, S. Harimoto, S. Onoue, H. Nomura and R. Nakatani: J. Appl. Phys. **117** (2015) 17D902.
18) Y. Shiratsuchi, Y. Kotani, S. Yoshida, Y. Yoshikawa, K. Toyoki, A. Kobane, R. Nakatani and T. Nakamura: AIMS Mat. Sci. **2** (2015) 484–496.
19) X. He, Y. Wang, N. Wu, A.N. Caruso, E. Vescovo, K.D. Belashchenko, P.A. Dowben and C. Binek: Nat. Mater. **9** (2010) 579–585.
20) T. Ashida, M. Oida, N. Shimomura, T. Nozaki, T. Shibata and M. Sahashi: Appl. Phys. Lett. **106** (2015) 132407.
21) S. Maat, K. Takano, S.S.P. Parkin and E.E. Fullerton: Phys. Rev. Lett. **87** (2001) 087202.
22) Z.Y. Liu: J. Magn. Magn. Mater. **281** (2004) 247–254.
23) C. Binek, B. Kagerer, S. Kainz and W. Kleemann: J. Magn. Magn. Mater. **226–230** (2001) 1814–1816.
24) N.H. Dung, N.P. Thuy, N.A. Tuan, N.T. Long and N.N. Phuoc: J. Magn. Magn. Mater. **320** (2008) 3334–3340.
25) F. Garcia, J. Sort, B. Rodmacq, S. Auffret and B. Dieny: Appl. Phys. Lett. **83** (2003) 3537–3539.
26) J. Sort, F. Garcia, B. Rodmacq, S. Auffret and B. Dieny: J. Magn. Magn. Mater. **272–276** (2004) 355–356.
27) X. Ji, H. Ju, D.E. McCready and K.M. Krishnan: J. Appl. Phys. **98** (2005) 116101.
28) S. van Dijken, M. Besnier, J. Moritz and J. M. D. Coey: J. Appl. Phys. **97** (2005) 10K114.
29) J. Sort, V. Baltz, F. Garcia, B. Rodmacq and B. Dieny: Phys. Rev. B **71** (2005) 054411.
30) Y.F. Liu, J.W. Cai and S.L. He: J. Phys. D Appl. Phys. **42** (2009) 115002.
31) H. Takahashi, M. Tsunoda and M. Takahashi: IEEE Trans. Magn. **48** (2012) 4347–4350.
32) Y. Shiratsuchi, H. Oikawa, S. Kawahara, Y. Takechi, T. Fujita and R. Nakatani: Appl. Phys. Express **5** (2012) 043004.
33) M. Tsunoda, Y. Tsuchiya, T. Hashimoto and M. Takahashi: J. Appl. Phys. **87** (2000) 4375–4388.
34) M. Takahashi and M. Tsunoda: J. Phys. D Appl. Phys. **35** (2002) 2365–2376.
35) K. Nishioka, C. Hou, H. Fujiwara and R.D. Metzger: J. Appl. Phys. **80** (1996) 4528–4533.
36) G. Choe and S. Gupta: Appl. Phys. Lett. **70** (1997) 1766–1768.
37) R.F.C. Farrow, R.F. Marks, S. Gider, A.C. Marley, S.S.P. Parkin and D. Dauri: J. Appl. Phys. **81** (1997) 4986–4988.
38) D. Lederman, J. Nogués and I.K. Schuller: Phys. Rev. B **56** (1997) 2332–2335.
39) K. Nishioka, S. Shigematsu, T. Imagawa and S. Narishige: J. Appl. Phys. **83** (1998) 3233–3238.
40) W.H. Meiklejohn and C.P. Bean: Phys. Rev. **105** (1957) 904–913.
41) Y. Shiratsuchi, T. Fujita, H. Noutomi, H. Oikawa and R. Nakatani: IEEE Trans. Magn. **47** (2011) 3909–3912.
42) S. Foner: Phys. Rev. **130** (1963) 183–197.
43) H. Ohldag, A. Scholl, F. Nolting, E. Arenholz, S. Maat, A.T. Young, M. Carey and J. Stöhr: Phys. Rev. Lett. **91** (2003) 017203.
44) H. Takahashi, Y. Kota, M. Tsunoda, T. Nakamura, K. Kodama, A. Sakuma and M. Takahashi: J. Appl. Phys. **110** (2011) 123920.
45) M. Tsunoda, H. Takahashi, T. Nakamura, C. Mitsumata, S. Isogami and M. Takahashi: Appl. Phys. Lett. **97** (2010) 072501.
46) C. Mitsumata, M. Tsunoda, H. Takahashi and A. Sakuma: EPL **99** (2012) 47006.
47) A.F. Andreev: JETP Lett. **63** (1996) 758–762.
48) K.D. Belashchenko: Phys. Rev. Lett. **105** (2010) 147204.
49) N. Wu, X. He, A.L. Wysocki, U. Lanke, T. Komesu, K.D. Belashchenko, C. Binek and P.A. Dowben: Phys. Rev. Lett. **106** (2011) 087202.
50) F. Nolting, A. Scholl, J. Stöhr, J.W. Seo, J. Fompeyrine, H. Siegwart, J.-P. Locquet, S. Anders, J. Lüning, E.E. Fullerton, M.F. Toney, M.R. Scheinfein and H.A. Padmore: Nature **405** (2000) 767–769.
51) T.J. Martin and J.C. Anderson: IEEE Trans. Magn. **2** (1966) 446–449.
52) M.H. Kryder, E.C. Gage, T.W. McDaniel, W.A. Challener, R.E. Rottemayer, G. Ju, Y.-T. Hsia and M.F. Erden: Proc. IEEE **96** (2008) 1810–1835.
53) Y. Shiota, T. Nozaki, F. Bonell, S. Murakami, T. Shinjo and Y. Suzuki: Nat. Mater. **11** (2011) 39–43.
54) G.S.D. Beach, C. Nistor, C. Knutson, M. Tsoi and J.L. Erskine: Nat. Mater. **4** (2005) 741–744.
55) T. Ono, H. Miyajima, K. Shigeto, K. Mibu, N. Hosoito and T. Shinjo: Science **284** (1999) 468–470.
56) D. Atkinson, D.A. Allwood, G. Xiong, M.D. Cooke, C.C. Faulkner and R.P. Cowburn: Nat. Mater. **2** (2003) 85–87.